


## Article

# Study on the Visualization of Transport and Crystallization of Salt Solution in Simulated Wall Painting

Wendi Yu <sup>1</sup>, Lu Yang <sup>1,\*</sup>, Jing Zhao <sup>2,\*</sup>  and Hongjie Luo <sup>2</sup><sup>1</sup> School of Cultural Heritage, Northwest University, Xi'an 710127, China; wendiyu@stumail.nwu.edu.cn<sup>2</sup> Shanghai Institute of Ceramics, Chinese Academy of Sciences, Shanghai 200050, China; hongjieluo@mail.sic.ac.cn

\* Correspondence: yanglu@nwu.edu.cn (L.Y.); zhaojing@mail.sic.ac.cn (J.Z.)

**Abstract:** The transport and crystallization processes of chromogenic 5.0% CuSO<sub>4</sub> solution in the supporting body and coarse plaster of simulated wall painting samples were observed. A scanning electron microscope and a self-designed double-layer surface contact internal pressure method were used to test, respectively, the micro-morphologies of salt crystals in different regions and the micro-forces on the contact surfaces during the spread and crystallization of water and salt solution. The results demonstrate that the salt crystals formed by the CuSO<sub>4</sub> solution on the surface of the simulated wall painting showed two different shapes: a salt belt formed by clustered crystals, and a layer of salt crust. The difference was speculated to be related to the crystals' growth conditions. The destructive effect of salt solution and salt crystals on wall paintings manifested itself by weakening the connectivity between different materials, and changing the volume and morphology of the wall paintings. Using the double-layer surface contact internal pressure method, the forces generated by the salt solution and salt crystals on the simulated wall paintings were demonstrated to be adsorption force, expansion force generated by the crystals' precipitation and growth, and suction force resulting from water loss and the shrinkage of crystals. The expansion force and suction force were not in a stable state, resulting in the contact surfaces continuously bending and stretching. Compared with pure water, salt solution can aggravate damage to the stability of wall paintings. This analysis of the transport, crystallization and micro-forces of a chromogenic salt solution in simulated wall painting samples can provide a scientific basis for studying the general patterns of damage caused by soluble salt to wall paintings during its transport and crystallization, and provide insight that can further the protection of cultural relics.

**Keywords:** chromogenic salt solution; simulated wall painting; transport and crystallization; micro-force



**Citation:** Yu, W.; Yang, L.; Zhao, J.; Luo, H. Study on the Visualization of Transport and Crystallization of Salt Solution in Simulated Wall Painting. *Crystals* **2022**, *12*, 351. <https://doi.org/10.3390/cryst12030351>

Academic Editors: José L. Arias

Received: 27 December 2021

Accepted: 2 March 2022

Published: 4 March 2022

**Publisher's Note:** MDPI stays neutral with regard to jurisdictional claims in published maps and institutional affiliations.



**Copyright:** © 2022 by the authors. Licensee MDPI, Basel, Switzerland. This article is an open access article distributed under the terms and conditions of the Creative Commons Attribution (CC BY) license (<https://creativecommons.org/licenses/by/4.0/>).

## 1. Introduction

Ancient murals are important historical treasures of great scientific and artistic value; they are not only precious sources for studying social production modes and lifestyles in various historical periods but also essential carriers indicating different national cultures. Nevertheless, owing to the complex composition of Chinese wall paintings, the migration, dissolution, and crystallization of salt solutions [1] gradually produces some serious forms of damage, including cracks, flaking, and detachment of the pigment layer, all of which put these ancient wall paintings at risk. For example, Figure 1 shows the efflorescence of Maiji Mountain Grottoes in China, built over 1600 years ago. Soluble salt solutions have caused the plaster layer to expand, the surface structure to be loosened, and plaster layer material to fall off [2].

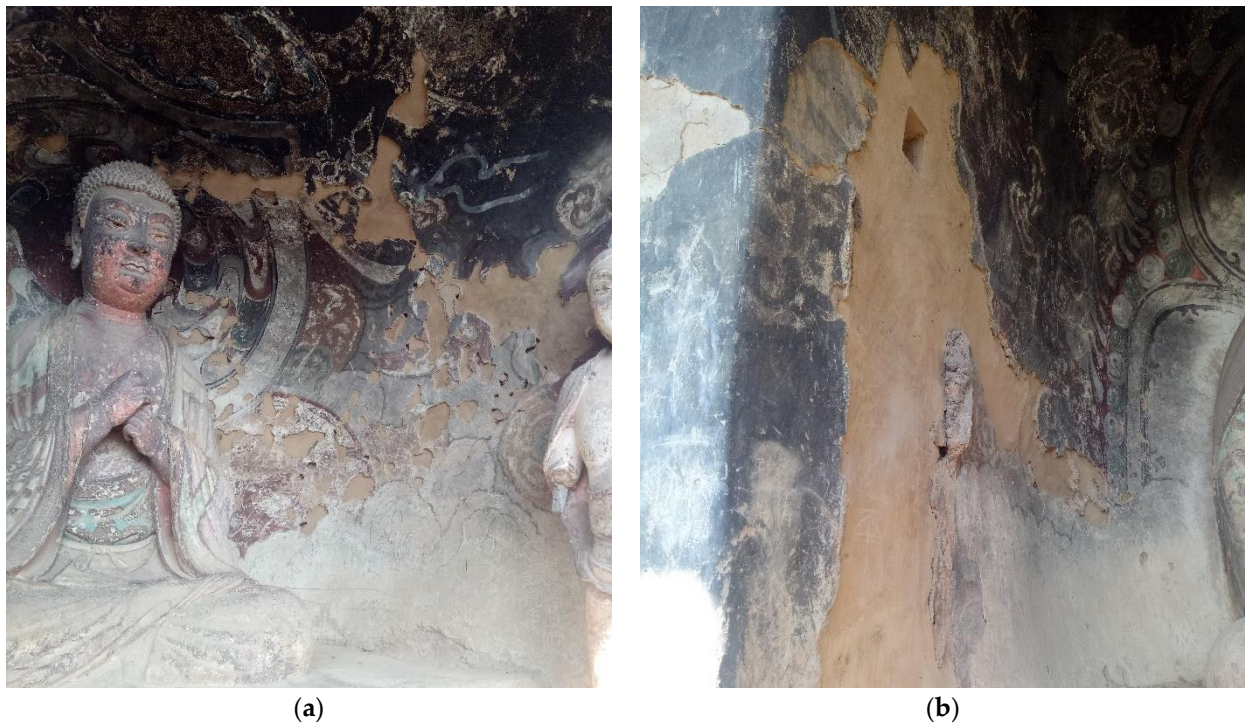


**Figure 1.** The efflorescence of Maiji Mountain Grottoes: detachment of the plaster layer (a,b).

At present, research on soluble salt solutions in wall paintings have mostly focused on the sources of water and salt [3–5], the mechanism of salt damage [6–18], detection of soluble salts, and methods of desalination [19–30]. Many researchers have analyzed the thermodynamic and kinetic mechanism and crystallization law of soluble salts in stone materials [31–38]. However, there is no clear study on micro-forces during the transport and crystallization of soluble salt solutions in wall paintings. There have been some studies on the migration and crystallization of salt solutions in porous samples [39–43]; however, these methods have certain flaws when applied to large cultural relics. Given that the surface tension and crystal mode of a  $\text{CuSO}_4$  solution are very similar to those of an  $\text{Na}_2\text{SO}_4$  solution contained in wall paintings [44], and that the chromogenic property of  $\text{CuSO}_4$  solution displays a similar process of change in wall painting samples more obviously [45], a 5.0%  $\text{CuSO}_4$  solution was selected for this study, and its transport and crystallization process in a simulated wall painting sample and simulated coarse plaster was observed. The microscopic morphologies of crystals were observed by means of a scanning electron microscope. Using a self-designed double-layer surface contact internal pressure method, the micro-forces generated by water and salt solution on the double-layered contact surfaces were tested during the spread, evaporation, and crystallization of the liquid. In addition, the micro-forces generated on the double-layer contact surfaces as a result of the coarse plaster containing water and a salt solution during liquid change were also tested.

## 2. Experimental Methods and Detection Techniques

### 2.1. Preparation of Simulated Wall Painting Samples

A complete wall painting generally includes three parts: the supporting body, the coarse plaster and the paint layer. Many Chinese wall paintings were made on sandstone and conglomerate [46]; therefore, a sandstone sample with high compressive strength was used to simulate the supporting body. In this experiment, Chinese sandstone with a calcium content of about 2% was selected. Its water absorption, apparent porosity, bulk density, and compressive strength were 4.93% by mass, 10.93%,  $2.22 \text{ g}\cdot\text{cm}^{-3}$ , and 49.20 MPa, respectively. The raw materials of the plaster layer were silt, sand, wheat straw, and fine linen. The “fine linen” we chose was jute sold in the northern markets of

China. The soil and sand used to make the coarse and fine plaster were screened with sieves, mixed with a certain amount of water, wheat straw, or fine linen, and stirred evenly. The proportion of soil, sand, wheat straw/fine linen, and water was about 48:27:2:23. We smeared a thick coarse plaster mixed with wheat straw onto the surface of the supporting body, then smeared on a thin fine plaster mixed with fine linen to make a smooth plane, and painted on a layer of white powder consisting of lime and water. Finally, traditional pigments commonly used in Chinese paintings, mixed with 5% gelatin, were painted onto the white powder layer to prepare the paint layer. The Chinese paint pigments we chose were various mineral pigments used in the Dunhuang murals [47], with a red pigment made of ochre, a green pigment made of malachite, a blue pigment made of azurite, and a black pigment made of pine-soot ink. The soil and sandstone used to make the sample was desalted beforehand [48]. We conducted many experiments and selected a representative sample for display. The size of the selected simulated wall painting sample was about  $5.5\text{ cm} \times 5.5\text{ cm} \times 5.3\text{ cm}$  (Figure 2). The profile of the sample is shown in Figure 3. To analyze the effect of the salt solution on the coarse plaster and paint layers, a 55.8 g sample consisting of coarse plaster and paint layers was also made in the same way as the sample described above.

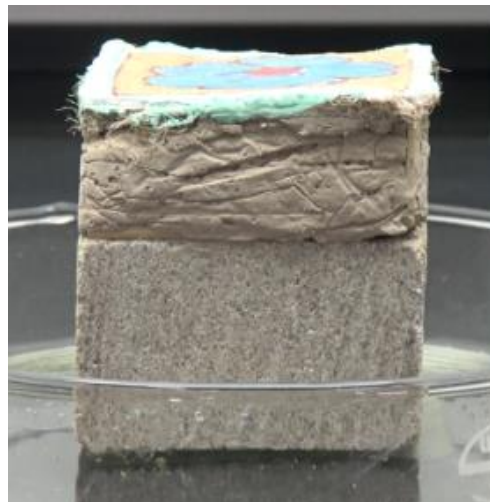


**Figure 2.** The simulated wall painting sample.

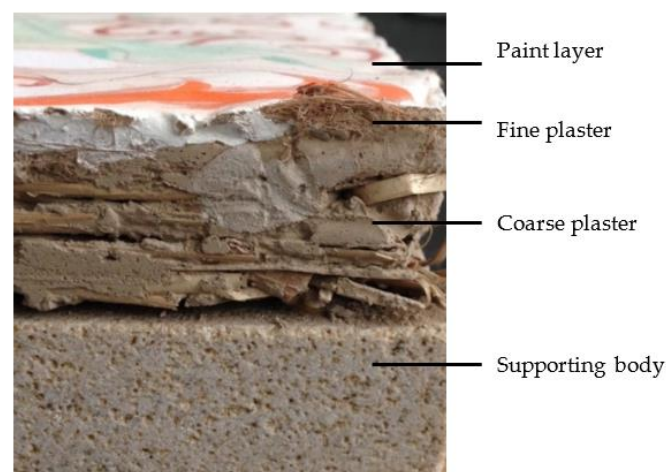


**Figure 3.** The profile of the sample.

## 2.2. Experimental Methods and Characterization of Results

### 2.2.1. Observation of the Transport and Crystallization of a Salt Solution in a Simulated Wall Painting Sample

A 5.0%  $\text{CuSO}_4$  solution was prepared (anhydrous copper sulfate crystal and deionized water, anhydrous copper sulfate crystal: AR, purity 99.0%, Shanghai Aladdin Biochemical Technology Co., Ltd., Shanghai, China). A video recorder (SONY FDR-AX45, Tokyo, Japan) was used to record the process of change in the solution as it passed through the simulated wall painting sample in real time. The rate at which the solution rose was calculated according to the change in liquid level. Meanwhile, changes in the salt crystals on the sample's surface and changes to the sample's volume caused by the salt solution were recorded. The controlled ambient temperature was 25 °C and the relative humidity was 50%.

### 2.2.2. Micromorphological Analysis of Crystals

After carbon plating the surface of salt crystals obtained by the evaporation of a 5.0%  $\text{CuSO}_4$  solution, the surface and section micro-morphologies of crystals forming the salt crust and salt belt were analyzed using a Jeol JSM-6700F (Akishima, Japan) scanning electron microscope.

### 2.2.3. Micro-Force Test

The controlled ambient temperature was 25 °C and the relative humidity was 50%. A self-designed double-layer surface contact internal pressure method was used to test the changes of force generated by water and the  $\text{CuSO}_4$  salt solution during its transport through the sample and the crystallization of the liquid. A Mettler Toledo ML203T/02 (Zurich, Switzerland) electronic balance was used to monitor the change in mass as the water and salt solution spread, evaporated, and crystallized within the double contact surfaces [49]. The diagram of the experimental device is shown in Figure 4. Surface 1 was a nonporous glass plate that cannot be penetrated or dissolved by the solution, and surface 2 was a porous plate with a pore width of about 1.0 mm and a pore spacing of about 1.0 mm that allowed water to evaporate via the pores. The specific operations included the following steps. The liquid was dropped onto contact surface 1; the value measured by the balance was the weight of the liquid. Contact surface 2 was quickly pressed onto the surface of the liquid, with the distance from contact surface 1 set to 1.0 mm. Since contact surfaces 1 and 2 were fixed, the change in mass measured by the balance related to the interaction between the liquid and the contact surfaces. For example, when the balance recorded negative figures, it meant that the upward force generated by the adsorption of the two contact surfaces and the liquid was greater than the gravity of the liquid itself. The absolute value of such negative values increased as the upward adsorption force increased. When the balance recorded positive figures, this indicated that an expansion force was being generated between the two contact surfaces due to the formation of crystals. The greater the expansion force, the greater the positive value displayed. These recorded changes in mass can be used to determine the change in forces during the processes of evaporation, crystal nucleus formation, crystal growth and complete crystallization of the solution. Moreover, the micro-forces on the double-layer contact surfaces generated by the coarse plaster's water and salt solution content during liquid changes were also tested.



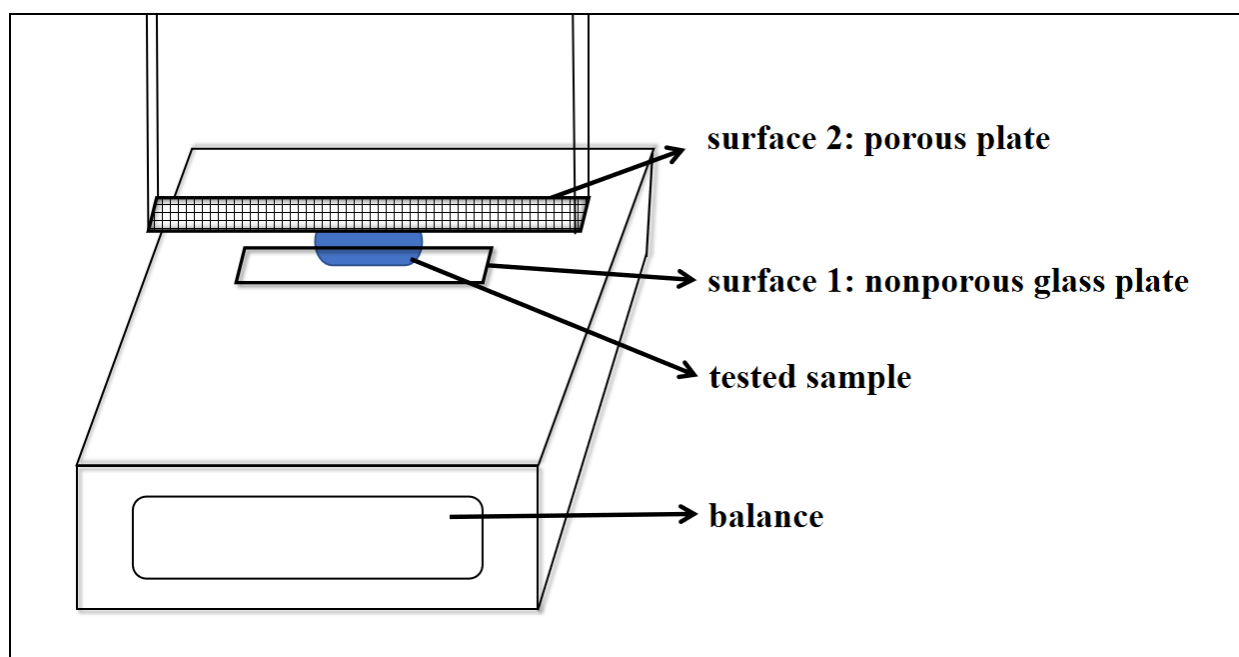


**Figure 4.** Diagram of experimental device using double-layer surface contact internal pressure method.

### 3. Results and Discussion

#### 3.1. Transport and Crystallization of the Salt Solution in the Simulated Wall Painting Sample

The sample was placed in a container containing  $\text{CuSO}_4$  solution, at a depth of about 1.0 cm. Changes in the salt solution within the simulated wall painting sample was recorded in real time. In the first 3.5 h, the rate of transport of the  $\text{CuSO}_4$  solution through the simulated wall painting sample was about  $0.57 \text{ mm} \cdot \text{h}^{-1}$ . When the salt solution had migrated upward by capillary action for 3.5 h—in other words, when the salt solution was at a height of about 2 mm from the solution level—salt crystals began to appear at the solid–liquid interface (Figure 5b). With the continuous accumulation of crystals, the rising rate of the solution became faster and the salt crystal content increased more in the corner region of the sample, which has more capillary pores and greater ambient airflow. When the salt crystals grew and accumulated in clusters at the interface between the supporting body and the coarse plaster at the edge of the sample (Figure 5c), the crystallization of the salt solution and the crystal growth produced a force on the coarse plaster, resulting in its micro-deformation (Figure 5d). The dynamic diagram of specific deformation process is shown in the Supplementary Material Figure S1. The molecular attraction and the surface tension at the interface generated by the solution and air, as well as the solution and the porous sample, caused the water to migrate to the sample's surface [45].

The salt belt on the surface of the simulated wall painting sample grew, accumulating upward and widening. In addition, a layer of salt crust covering the sample's surface formed between the solution's surface and the salt belt, as shown in Figure 5. After 120 h, with the continuous decrease in the delivery of salt solution, the level of liquid solution decreased, and the salt crust on the sample surface crystallized and dried. If any errors caused by the non-uniformity of the rock are ignored, we can say that the crystals always rose higher at the sample's edges (Figure 6), forming an inverted parabolic shape [45].

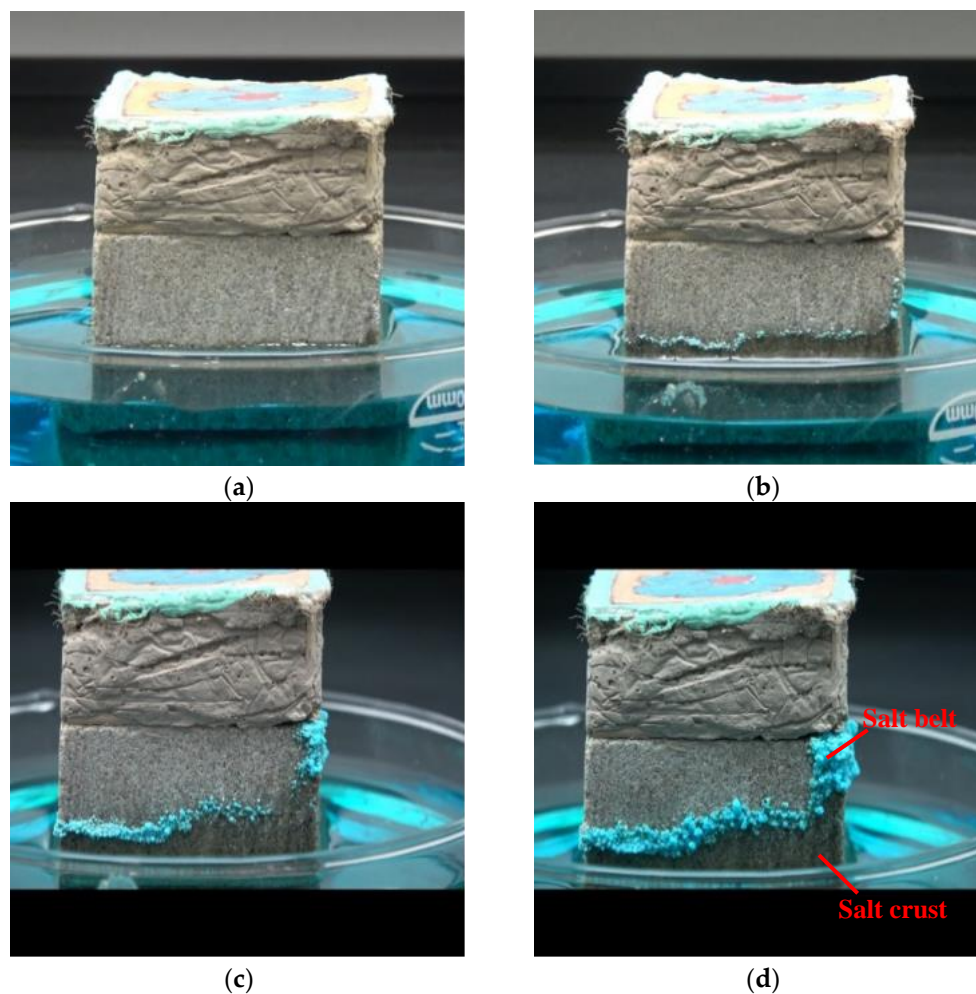


**Figure 5.** The transport and crystallization process of salt solution in the simulated wall painting sample (a) 0 h; (b) 7 h; (c) 36 h; (d) 72 h.

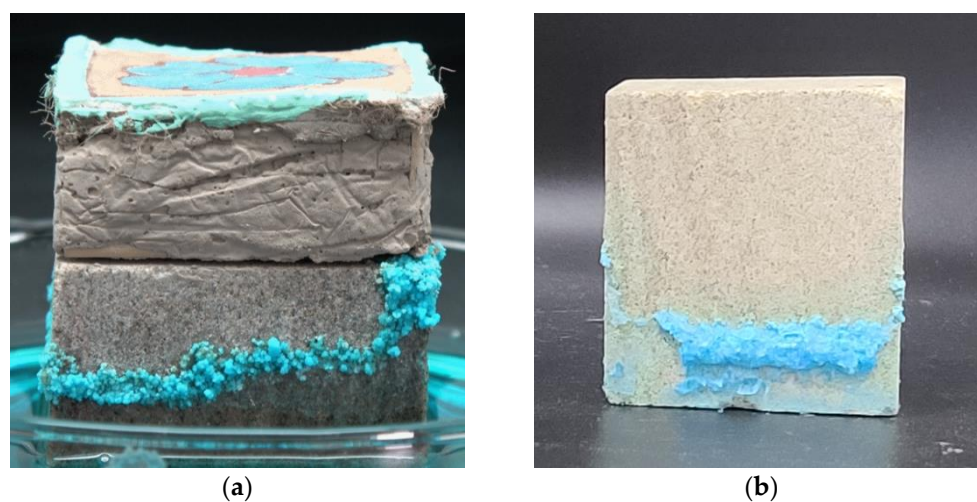


**Figure 6.** Inverted parabolic shapes formed by crystals (a) salt belt on the sample shot from a different angle; (b) another simulated sample whose bottom was soaked with less salt solution.

The micro-morphologies of clustered salt crystals (Figure 7) and crystals forming the salt crust (Figure 8) were tested by means of SEM. As shown in Figure 7, it was found that the clustered crystals were larger at the edges and corners because these areas could

more easily accept the solute and the crystals grew faster there. The clustered crystals presented a ladder accumulation of particles 1.25–5.00  $\mu\text{m}$  in size. However, the size of crystals forming the salt crust in Figure 8 was smaller, relatively speaking. The crust was mainly composed of 0.01–0.50  $\mu\text{m}$  particles which formed a lamellar accumulation with a thickness of about 3–5  $\mu\text{m}$ .

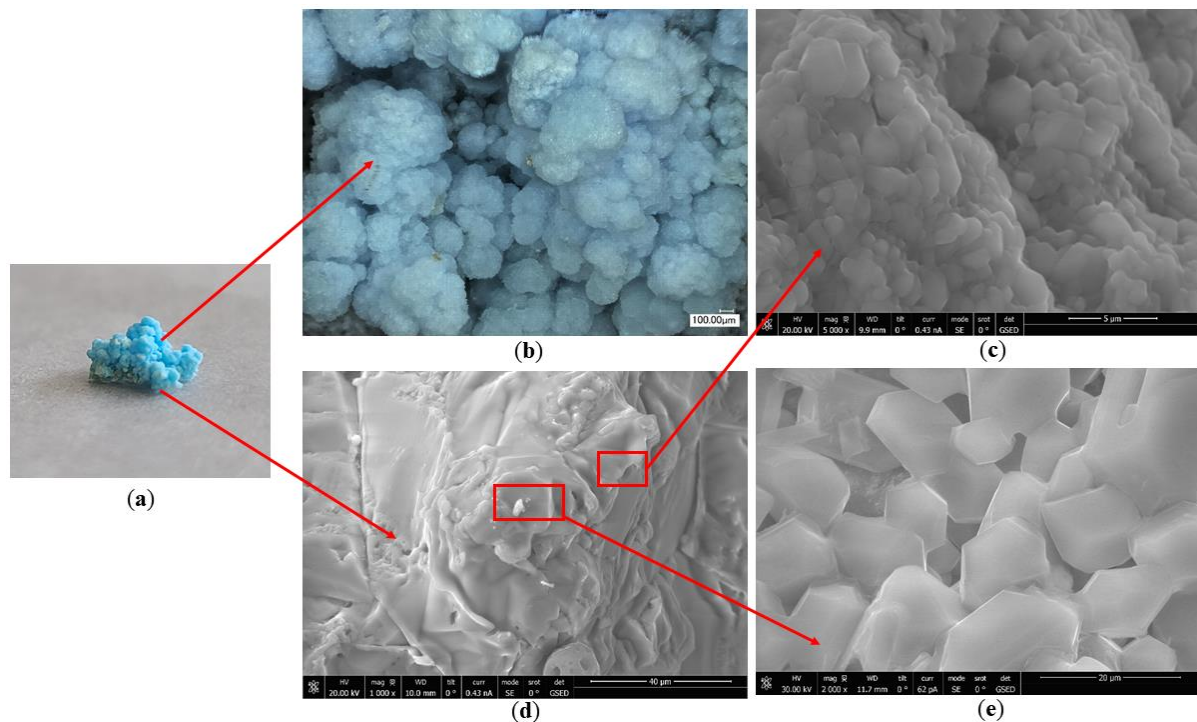


**Figure 7.** Photos of clustered salt crystals (a) crystals collected from the salt belt; (b) clustered crystals (c) top of clustered crystals; (d) side of clustered crystals; (e) micro-morphology of the crystals.

According to the test results, the difference in crystal morphology between the clustered salt belt and the lamellar salt crust related to the growth conditions. Due to the decrease in moisture content at the pore level, when the unsaturated capillary flow is no longer able to supply water, a certain amount of salt will crystallize at each cluster [50]. The salt solution continued to flow upward along the salt belt on the surface, resulting in larger crystal sizes and continuous widening of the salt belt. It is speculated that the process of forming clustered salt crystals relates to the eddies in the motion of the salt solution in the sample. Around the growing crystals, the solute in the solution adhered to them, leading to a decrease in the solution's concentration. In addition to the heat released by the crystals' growth, the solution's density decreased. Under the action of gravity, the water rose and the salt solution was continuously replenished; the upward eddy motion produced by crystallization eventually led to the upward widening of the salt belt. There were different crystallization rates: the solution in the salt belt had a fast crystallization rate and many crystallization centers. Further, under the action of the unsaturated solution, the crystals dissolved and recrystallized. A single crystal was approximately spherical, and the stacked crystals were dendritic. The upward stacking of salt crystals is also related to the creeping effect [51].

Between the liquid surface of the salt solution and the formed salt belt, the solute was easily obtained below the salt belt's crystals, forming a lamellar salt crust which was attached to the sample's surface and grew downwards (Figure 8). Due to the continuous decrease in the liquid level of the salt solution and the changes in ion concentration, cracks formed between each layer of crystals; these can be directly observed in the cross-sectional morphology of the salt crust in Figure 8. In addition, the formed crust itself can act itself as a porous medium, building up additional layers of salt crystals [52].



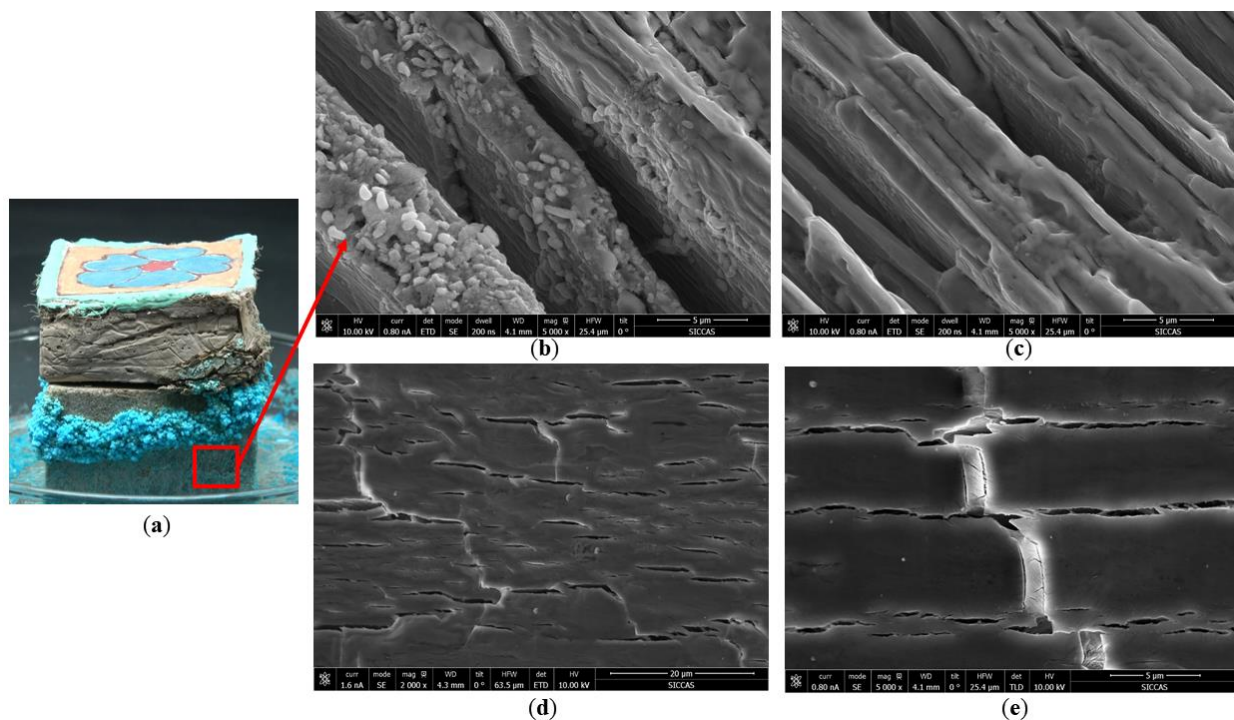


**Figure 8.** Images of crystals forming the salt crust (a) salt crust on the surface; (b) SEM salt crust photo; (c) SEM salt crust photo in another location; (d) cross-sectional morphology of the salt crust, 1000 $\times$ ; (e) cross-sectional morphology of the salt crust, 5000 $\times$ .

The forces generated by the salt belt's formation on the surface of the simulated wall painting sample were analyzed, but the specific role of each component in the deformation dynamics wasn't been studied in depth. The transport of the salt solution through the porous sample was mainly due to capillary action. In the process of crystallization, the location and width of the salt belt were determined by patterns in the capillary transport of the salt solution, the laminar flow of water through the pores, and the concentration of the salt solution [44]. The crystallization force at the interface between the supporting body and the coarse plaster directly determined the degree of damage suffered by the sample. The crystallization force of the salt solution widened the split between the supporting body and the coarse plaster and weakened their connectivity.

### 3.2. Transport and Crystallization of a Salt Solution in the Simulated Coarse Plaster and Paint Layers

Taking into consideration the substantial difference in composition between the supporting body and other parts of the simulated wall painting sample, after analyzing the movement and change in the salt solution in the supporting body, the experiment further observed the transport and crystallization process of the salt solution through the coarse plaster and paint layers. A 55.8 g sample was selected, consisting of the coarse plaster and paint layers and 8.0 g of the 5.0%  $\text{CuSO}_4$  solution was added. The changes in sample volume and surface morphology during absorption solution and complete drying were recorded in real time.

The size and morphology of the paint layer on the surface of the simulated wall painting sample (Figure 9) remained almost unchanged due to the bonding effect of the binder. However, the volume of the coarse plaster expanded, and there was warping of the paint layer, especially at the edges that were in contact with the coarse plaster. The morphology of the sample changed from an initial cylinder to an irregular round platform (Figure 9d).



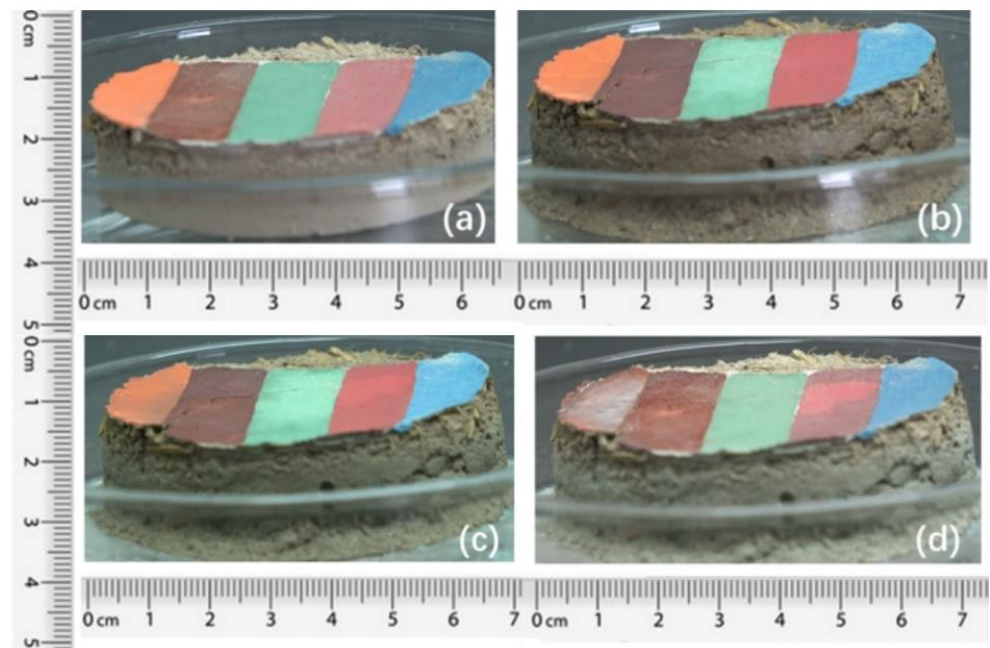


**Figure 9.** The processes of change as the sample consisting of coarse plaster and paint layers absorbed the solution then dried out: (a) untreated sample; (b) after absorbing salt solution for 54 min; (c) after losing water and shrinking for 6 h; (d) after drying for 30 h.

Our analysis showed that the coarse plaster changed in three stages: absorbing salt solution, losing water and shrinking, and drying out. In the first stage, the volume of the sample expanded continuously after absorbing the salt solution. As can be seen by comparing the coarse plaster in Figure 9a,b, the sample changed in both horizontal and vertical dimensions, from an initial base diameter of 6.5 cm and height of 1.5 cm to a diameter of 7.0 cm and height of 2.0 cm, although the diameter of the top was almost unchanged. The volume expansion rate was about 43.85%. In the second stage, after the sample had absorbed the solution for 54 min and reached its maximum volume expansion, it began to lose water, resulting in volume shrinkage. After about 6 h, the height changed from 2.0 cm to 1.9 cm before salt crystals were precipitated on the surface. The volume shrinkage was about 5.00%. In the third stage, the crystals of cupric sulfate pentahydrate were continuously precipitated on the surface, and the volume of the sample did not change after about 30 h. As shown in Figure 9c,d, the diameter of the coarse plaster changed from 7.0 cm to 7.1 cm and its height decreased from 1.9 cm to 1.7 cm. The volume shrinkage rate was about 9.18%, with the base diameter widening and the height decreasing. Compared with the initial cylindrical sample shown in Figure 9a, and the irregular round platform in the stable state of dehydration shown in Figure 9d, the overall expansion rate was about 24.18%.

The change in size and stress caused by the salt solution can weaken the connection between the paint layer and the coarse plaster, and may even cause the paint layer to warp and fall off.

### 3.3. Micro-Forces Generated by the Salt Solution in the Changing Process

The changes in the salt solution caused changes in the shape and volume of the simulated wall painting samples, and the micro-forces generated as a result of these processes of change in the solution were tested using the self-designed double-layer contact surface internal pressure method described above.

### 3.3.1. Micro-Forces Generated by the Salt Solution

A total of 0.50 g deionized water was weighed out and placed on surface 1 of the of double-layer surface contact internal pressure experimental device (as shown in Figure 4). The distance between the double-layer contact surfaces was set to 1.0 mm and the contact surfaces were in full contact with the water surface; changes in mass were measured using the balance throughout the process. The results are shown as the black curve in Figure 10a. In stage a, the liquid attached to the double-layer contact surfaces. When the upward force generated by the adsorption of the two contact surfaces and the liquid was greater than the gravity of the liquid itself, the balance displayed a negative value. With the liquid's spread, adsorption gradually increased. The absolute value of the negative value increased as the upward adsorption force increased. After reaching its maximum value, the water began to evaporate, and the force on the double-layer contact surfaces gradually decreased, indicated by the gradual increase in the mass curve (stage b). After about 11 h, the water had completely evaporated and the interaction force on the double-layer contact surfaces disappeared completely.

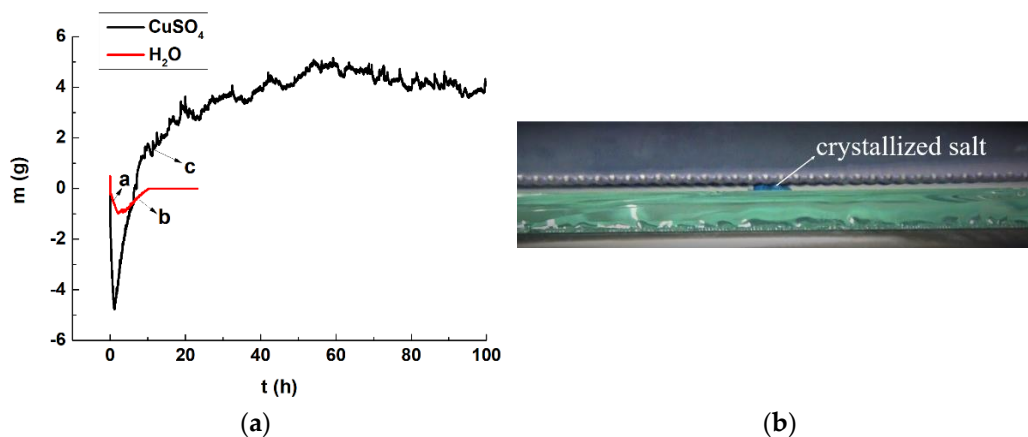


**Figure 10.** The change in mass of the salt solution and water tested by the double-layer contact surface internal press method (a) mass change curves; (b) crystallized salt.

A 5.0%  $\text{CuSO}_4$  solution of the same mass was weighed out between the double-layer contact surfaces and the change in mass as the solution crystallized was measured, as shown by the red curve in Figure 10a. The changes observed during stage a were the same as those observed with the water, which is to say, the adsorption force produced by the water molecules on the double-layer contact surfaces increased with the spread of the solution's surface. Due to the evaporation of the water in the solution, after about 7 h, the solution was supersaturated and crystals precipitated continuously, generating an expansion force on the two contact surfaces. The solution continued to evaporate and the crystals grew, as shown by the continuous rise in the mass curve. The downward part of the mass curve is mainly due to the dehydration and drying out of the deliquescent crystals, which increased the suction force between the double-layer contact surfaces; this force was mainly generated by shrinkage of the crystals. After point c on the graph, the curve indicates a process of continuous decreases and increases, which are due to the continuous crystallization and deliquescence of the crystals, causing the mass to increase due to water evaporation and decrease due to deliquescence. The changes in force generated by the copper sulfate solution's crystallization are similar to those generated by sodium sulfate solution, according to a previous study using the double-layer surface contact internal pressure method [49]. The solute content of the 0.5 g solution was measured and found to be 0.025 g. The greatest weight displayed on the balance was about 5.0 g, indicating that the force generated by the salt crystals plus the gravity of the salt crystals themselves was about  $0.005 \text{ kg} \times 9.8 \text{ N/kg}$ . However, the weight of the salt crystals was relatively small, meaning it can be ignored.

Comparing the changes in mass of the water and salt solution, it can be seen that the solution's molecules produced an adsorption force on the double-layer contact surfaces. The forces produced by the salt solution included an expansion force, caused by the growth of salt crystals on the double-layer contact surfaces, and a suction force generated when the crystals lost water and shrank. Due to the continuous crystallization–deliquescence of the crystals, the forces they generated were not constant, leading a continuously changing process of bending and stretching of the contact surfaces. It can be inferred that the presence of a salt solution inside wall paintings may generate unstable forces of the same nature on the pores.

### 3.3.2. Micro-Forces Generated by the Salt Solution in Coarse Plaster

After placing the coarse plaster sample on the surface 1 and returning the balance value to zero, 9.0 g liquid was dropped onto the coarse plaster; the value measured by the balance was therefore the weight of the salt solution. The surface 2 was put in complete contact with the liquid surface. Changes in mass of the coarse plaster were tested with water and with the salt solution; the results are shown in Figure 11. The water was first adsorbed into the upper contact surface and it was observed that the adsorption force increased with the continuous spread of water, which is shown in the stage a curve in Figure 11a. Due to the expansion in volume of the coarse plaster as it absorbed water, when the upper surface of the plaster touched the surface 2, it generated an expansion force on the surface, causing the value displayed on the balance to increase, as shown in the stage b curve in Figure 11a. The stage b curve rises and remains stable for about 3000 min. As the coarse plaster gradually dried out, its volume shrank again, causing the force generated on the contact surface to gradually decrease, as shown by the gradual decrease in the value measured by the balance. The c curve in Figure 11a shows that the sample gradually lost water, with almost complete loss after 1000 min, after which the mass of the sample remained stable.

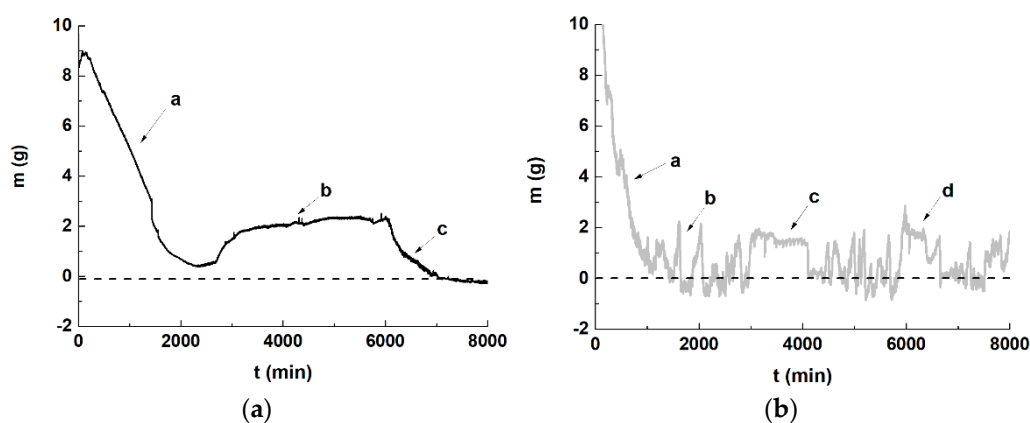


**Figure 11.** The mass change curves of the water-containing coarse plaster and salt-containing coarse plaster tested by double-layer surface contact internal pressure method (a) water-containing coarse plaster; (b) salt-containing coarse plaster.

Consistent with the laws governing changes in water-containing samples, the mass curve of the salt-containing sample decreased continuously as the salt solution spread, increased after the solution was absorbed and the sample expanded, and began to decrease as the solution evaporated. The difference was that the change in the mass of the salt solution was unstable, as reflected by the curve; that is, the force generated on the double-layer plates was unstable due to the changes occurring in the salt solution. In stage b in Figure 11b, the continuous process of crystallization and deliquescence of crystals is indicated by the burred rising and falling shape of the curve, with changes occurring faster than during the expansion in volume caused by the sample's absorption of the solution. After the volume had been stable for about 1000 min (stage c) it started to shrink, and then



expand again (stage d); from this point the curve begins to rise and fall again, generating a burred shape. This indicates the process of “crystals’ crystallization and deliquescence” and “sample’s expansion and shrinkage” alternately changed. It is speculated that this is related to discontinuity in the laminar flow of the solution in the sample, which is accelerated by the crystallization–deliquescence of the salt crystals. Due to the anisotropic nature of the materials used in wall paintings, compared with pure water, salt solutions can aggravate the destruction of the bonding between different materials.

#### 4. Conclusions

The transport and crystallization process of a 5.0% CuSO<sub>4</sub> solution in simulated wall painting samples was observed. The microscopic morphologies and micro-forces generated by crystals were tested by means of a scanning electron microscope and a self-designed double-layer surface contact internal pressure method. The results showed that:

- (1) Chromogenic CuSO<sub>4</sub> solution formed two different shapes: a salt belt formed by clustered crystals and a salt crust layer below the salt belt. In the salt belt, the clustered crystals were larger in size, mainly presenting a ladder accumulation of 1.25–5.00 µm particles. The size of the crystals forming the salt crust were smaller, mainly particles of 0.01–0.50 µm, presenting a lamellar accumulation with a thickness of about 3–5 µm. It is speculated that the differences in crystal morphology are related to the growth conditions.
- (2) The crystallization of the salt solution in the simulated wall painting sample weakened the bonding between the supporting body and the coarse plaster, resulting in the micro-deformation of the coarse plaster. Furthermore, the effect of the salt solution on the sample consisting of coarse plaster and a paint layer resulted in changes in the appearance change of the sample, from an initial cylinder to an irregular round table. The maximum expansion rate was about 43.85%, and the overall expansion rate was about 24.18%.
- (3) The double-layer surface contact internal pressure method showed that the main forces generated by the salt solution were an expansion force on the contact surfaces during crystallization and crystal growth, and a suction force generated when the crystals lost water and shrank. The expansion and suction forces were not stable and led to the contact surfaces continuously bending and stretching. Under the controlled experimental conditions, the maximum force on the double-layer surfaces reached about 0.049 N when the content of the solute was 0.025 g.
- (4) The process of “crystals’ crystallization and deliquescence” and “sample’s expansion and shrinkage” alternately changed. This was inferred to be related to the laminar flow of the solution in the sample, with the crystallization deliquescence of the salt solution accelerating the discontinuity in laminar flow. Due to the anisotropic nature of the materials used in wall paintings, compared with pure water, salt solutions can aggravate the loss of connectivity between different materials.

This analysis of the transport, crystallization, and micro-forces associated with the penetration of a chromogenic salt solution into simulated wall painting samples can provide a scientific basis for studying the general laws governing damage caused by soluble salts to wall paintings during transport and crystallization, contributing to the further protection of cultural relics.

**Supplementary Materials:** The following supporting information can be downloaded at: <https://www.mdpi.com/article/10.3390/cryst12030351/s1>, Figure S1. Dynamic change process of salt solution in simulated sample.

**Author Contributions:** Data analysis, W.Y.; methodology, J.Z. and H.L.; writing—original draft preparation, W.Y.; writing—review and editing, L.Y. and J.Z.; funding acquisition, H.L. and J.Z. All authors have read and agreed to the published version of the manuscript.

**Funding:** This work was supported by the Key Program of the National Natural Science Foundation of China (51732008) and National Natural Science Foundation of Shanghai in China (20ZR1422800).

**Institutional Review Board Statement:** Not applicable.

**Informed Consent Statement:** Not applicable.

**Data Availability Statement:** Data are available from the corresponding author on request.

**Conflicts of Interest:** The authors declare no conflict of interest.

## References

1. Ma, H. A summary of the influence of salt on ancient murals. *Identif. Apprec. Cult. Relics* **2022**, *22*, 63–65. [\[CrossRef\]](#)
2. Yue, Y.Q. Condition Surveys of Deterioration and Research of Wall Paintings in Maijishan Cave-temple. *Res. Herit. Preserv.* **2019**, *4*, 127–131. [\[CrossRef\]](#)
3. Yu, Z.R.; Wang, Y.W.; Wang, X.W.; Zhao, L.Y.; Guo, Q.L.; Wang, X.D. Research on the Water Vapor Source Induced Diseases of Wall Paintings in Longxing Temple. *Adv. Earth Sci.* **2017**, *32*, 668–676. [\[CrossRef\]](#)
4. Wang, J.F. Salt deterioration and soluble salt characteristics of porous materials. *Gansu Sci. Technol.* **2011**, *27*, 55–58. [\[CrossRef\]](#)
5. Su, Z.Y.; Yang, B.Z.; Zhang, H.Y. Soluble salt distribution and environmental monitoring of Cave 276 in the Mogao Grottoes. *J. Lanzhou Univ. Nat. Sci.* **2021**, *57*, 226–232. [\[CrossRef\]](#)
6. Li, F.J.; Wang, X.D.; Guo, Q.L. Adsorbed Moisture Feature and Suction Variation Characteristics of Earthen plaster in Mogao Grottoes under Influence of Humidity. *J. Eng. Geol.* **2021**, *29*, 1188–1198. [\[CrossRef\]](#)
7. Zhao, J.; Luo, H.J.; Huang, X. Migration, Distribution, and Crystallization of NaCl and Na<sub>2</sub>SO<sub>4</sub> Solutions in Three Different Media. *Crystals* **2020**, *10*, 444. [\[CrossRef\]](#)
8. Zheng, Z.H. Experimental investigation on state transform of sodium sulfate and its damaging effect on ancient mural in tomb of Princess Yongtai. *J. Nat. Disasters* **2020**, *29*, 158–163. [\[CrossRef\]](#)
9. Godts, S.; Hayen, R.; De Clercq, H. Investigating salt decay of stone materials related to the environment, a case study in the St. James church in Liege, Belgium. *Stud. Conserv.* **2017**, *62*, 329–342. [\[CrossRef\]](#)
10. Wang, J.L.; Zhang, Y.D.; Wu, Y.Q.; Liu, H.L.; Wang, X.D. Influence of Salt/Water Ratio on Emergence and Developing Rate of Mural Disruption. *Surf. Technol.* **2017**, *46*, 1–7. [\[CrossRef\]](#)
11. Roberto, G.; Elena, M.M.; Mariano, C.; Emanuele, C. Deterioration of building materials and artworks in the ‘Santa Maria della Stella’ church, Saluzzo (Italy): Causes of decay and possible remedies. *Stud. Conserv.* **2017**, *62*, 474–493. [\[CrossRef\]](#)
12. Jin, Z.L.; Liu, D.D.; Zhang, Y.K.; Chen, G.Q.; Xia, Y.; Su, B.M.; Zhou, T.; Lv, G.X.; Luo, H.J. Salt migrations and damage mechanism in cultural heritage objects. *Sci. Conserv. Archaeol.* **2017**, *29*, 102–116. [\[CrossRef\]](#)
13. Jin, Z.L.; Chen, G.Q.; Qian, L.; Su, B.M.; Lv, G.X. Study on the mechanism of salt damages on the mural paintings of mogao grottoes. *Chem. Res. App.* **2009**, *21*, 450–454. [\[CrossRef\]](#)
14. Jin, Z.L.; Chen, G.Q.; Qian, L.; Su, B.M.; Lv, G.X. Study on salt damage mechanism of murals in Mogao Grottoes (I). *Dunhuang Res.* **2008**, *6*, 50–53. [\[CrossRef\]](#)
15. Jin, Z.L.; Chen, G.Q.; Qian, L.; Su, B.M.; Lv, G.X. Study on salt damage mechanism of murals in Mogao Grottoes (II). *Dunhuang Res.* **2009**, *3*, 100–102. [\[CrossRef\]](#)
16. Jin, Z.L.; Chen, G.Q.; Xia, Y.; Su, B.M.; Zhou, T.; Lv, G.X. Comparative study of salt damage caused by sulfates and chlorides to mural paintings—Evidence of superpenetration, migration and crystallization destruction resulting from sodium sulfate. *Sci. Conserv. Archaeol.* **2015**, *21*, 29–38. [\[CrossRef\]](#)
17. Wang, Y.J.; Yu, Q.L.; Yan, M.; Ma, L.Y.; Chen, G.Q. Research on the mobility of soluble salts for north temple murals. *Sci. Conserv. Archaeol.* **2010**, *22*, 15–20. [\[CrossRef\]](#)
18. Su, B.M. Salt damage and daily maintenance of Dunhuang wall paintings. *Dunhuang Res.* **2010**, *6*, 14–16. [\[CrossRef\]](#)
19. Vettori, S.; Bracci, S.; Cantisani, E.; Riminesi, C.; Sacchi, B.; D’Andria, F. A multi-analytical approach to investigate the state of conservation of the wall paintings of Insula 104 in Hierapolis (Turkey). *Microchem. J.* **2016**, *128*, 279–287. [\[CrossRef\]](#)
20. Moussa, A.M.A.; Kantiranis, N.; Voudouris, K.S.; Stratis, J.A.; Christmas, M.F.A. The impact of soluble salts on the deterioration of pharaonic and coptic wall paintings at Al Qurna, Egypt: Mineralogy and chemistry. *Archaeometry* **2009**, *51*, 292–308. [\[CrossRef\]](#)
21. Raphael, A.J.W.; Christian, S. The Origin of Soluble Salts in Rocks of the Thebes Mountains, Egypt: The Damage Potential to Ancient Egyptian Wall Art. *J. Archaeol. Sci.* **2000**, *27*, 1161–1172. [\[CrossRef\]](#)
22. Chen, G.Q.; Hu, H.Y.; Li, Y.F.; Li, Z.; Jin, Z.L.; Qian, L.; Shui, B.W.; Lv, G.X. Micro-morphology and Composition of Mural Herpes in Mogao Grottoes. *Surf. Technol.* **2016**, *45*, 162–167. [\[CrossRef\]](#)
23. Rong, Y.; Li, Y.H.; Wang, B.D. Study on damaged situation of the Xigou No.4 and No.5 tombs in Jiuquan. *J. Shaanxi Norm. Univ. Nat. Sci.* **2015**, *43*, 47–52. [\[CrossRef\]](#)
24. Olmi, R.; Bini, M.; Ignesti, A.; Priori, P.; Riminesi, C.; Felici, A. Diagnostics and monitoring of frescoes using evanescent-field dielectrometry. *Meas. Sci. Technol.* **2006**, *17*, 2281–2288. [\[CrossRef\]](#)
25. Wei, R.; Liu, C. Investigation and analysis of soluble salt in architectural wall paintings of Fengguo temple in Liaoning Province. *Identif. Apprec. Cult. Relic* **2018**, *13*, 92–93. [\[CrossRef\]](#)

26. Li, J.M.; Tao, L.Y.; Zhang, B.J.; Zhang, H.; He, X.; Fan, Z.X.; Su, B.M. Laboratory simulation of the process of soluble salt damage to ancient grotto murals. *Sci. Conserv. Archaeol.* **2014**, *26*, 37–45. [\[CrossRef\]](#)
27. Du, H.Y.; Zhou, L.; Su, B.M.; Hu, Z.D. Rapid detection and analysis of salt damage in Dunhuang murals by capillary electrophoresis. *Dunhuang Res.* **2009**, *6*, 44–49. [\[CrossRef\]](#)
28. Zhou, L.; Du, H.Y.; Chen, G.Q.; Su, B.M.; Hu, Z.D. Growth Process & Features and Influencing Factors on Gully of The No. 4 Tomb in The Western Xia Mausoleums. *Dunhuang Res.* **2009**, *6*, 50–54. [\[CrossRef\]](#)
29. Su, B.M.; Chen, G.Q.; Fan, Z.X.; Ma, J.T.; Kang, H.W.; Li, R. The Application Research of a New Synthesized Desalination Material on the Treatment of Salting Damage Wall Paintings in Mogao Grottoes. *Relics Museol.* **2009**, *6*, 175–183. [\[CrossRef\]](#)
30. Chen, G.Q.; Fan, Z.X.; Yu, Q.L.; Su, B.M.; Li, Y.F.; Qiao, H.; Tang, W. Primary Test of Desalination to Treat the Disrupted Wall Painting in Cang Jie Temple of Baishui, Shaanxi Province. *Dunhuang Res.* **2009**, *6*, 8–12. [\[CrossRef\]](#)
31. Zehnder, K.; Arnold, A. Crystal growth in salt efflorescence. *J. Cryst. Growth.* **1989**, *97*, 513–521. [\[CrossRef\]](#)
32. Espinosa-Marzal, R.M.; Scherer, G.W. Advances in understanding damage by salt crystallization. *Acc. Chem. Res.* **2010**, *43*, 897–905. [\[CrossRef\]](#) [\[PubMed\]](#)
33. Derluyn, H.; Saidov, T.A.; Espinosa-Marzal, R.M.; Pel, L.; Scherer, G.W. Sodium sulfate heptahydrate I: The growth of single crystals. *J. Cryst. Growth.* **2011**, *329*, 44–51. [\[CrossRef\]](#)
34. Espinosa-Marzal, R.M.; Scherer, G.W. Impact of in-pore salt crystallization on transport properties. *Environ. Earth. Sci.* **2013**, *69*, 2657–2669. [\[CrossRef\]](#)
35. Shahidzadeh-Bonn, N.; Rafai, S.; Bonn, D.; Wegdam, G. Salt Crystallization during Evaporation: Impact of Interfacial Properties. *Langmuir* **2008**, *24*, 8599–8605. [\[CrossRef\]](#)
36. Tamerlan, A.S.; Pel, L.; Kopinga, K. Crystallization Pressure of Sodium Sulfate Heptahydrate. *Cryst. Growth Des.* **2015**, *15*, 2087–2093. [\[CrossRef\]](#)
37. Steiger, M. Crystal growth in porous materials I: The crystallization pressure of large crystals. *J. Cryst. Growth* **2005**, *282*, 455–469. [\[CrossRef\]](#)
38. Steiger, M. Crystal growth in porous materials II: Influence of crystal size on the crystallization pressure. *J. Cryst. Growth* **2005**, *282*, 470–481. [\[CrossRef\]](#)
39. Katz, A.J.; Thompson, A.H. Prediction of rock electrical conductivity from mercury injection measurements. *J. Geophys. Res.* **1987**, *92*, 599–607. [\[CrossRef\]](#)
40. Pel, L.; Kopinga, K.; Kaasschieter, E.F. Saline absorption in calcium silicate brick observed by NMR scanning. *J. Phys. D Appl. Phys.* **2000**, *33*, 1380–1385. [\[CrossRef\]](#)
41. Cano, F.D.; Bremner, T.W.; McGregor, R.P.; Balcom, B.J. Magnetic resonance imaging of  $^1\text{H}$ ,  $^{23}\text{Na}$ , and  $^{35}\text{Cl}$  penetration in Portland cement mortar. *Cem. Concr. Res.* **2002**, *32*, 1067–1070. [\[CrossRef\]](#)
42. Ruiz-Agudo, E.; Mees, F.; Jacobs, P.; Rodriguez-Navarro, C. The role of saline solution properties on porous limestone salt weathering by magnesium and sodium sulfates. *Environ. Geol.* **2007**, *52*, 269–281. [\[CrossRef\]](#)
43. Pel, L.; Pishkari, R.; Casti, M. A simplified model for the combined wicking and evaporation of a NaCl solution in limestone. *Mater. Struct.* **2018**, *51*, 66. [\[CrossRef\]](#)
44. Zhao, J.; Luo, H.J.; Huang, X. Migration, Crystallization and Dissolution Changes of Salt Solution with Color Rendering Property in Porous Quartz Materials. *Molecules* **2020**, *25*, 5708. [\[CrossRef\]](#)
45. Zhao, J.; Luo, H.J.; Huang, X. CuSO<sub>4</sub> chromogenic tracing for migration and crystallization of salt solution in porous materials. *J. Cryst. Growth* **2021**, *559*, 126040. [\[CrossRef\]](#)
46. Wang, C.Y.; Li, M.; Xia, Y.; Fu, Q.L.; Wang, W.F.; Jin, H.B. Study on the making technology of ancient Chinese grotto murals. *Relics Mus.* **2014**, *4*, 74–78. [\[CrossRef\]](#)
47. Xu, W.Y.; Zhou, G.X.; Li, Y.H. X-ray analysis report on inorganic pigments of murals and color sculptures in Mogao Grottoes. *Dunhuang Res.* **1983**, *3*, 187–197.
48. Ministry of Water Resources of the People's Republic of China. GB/T 50123-1999; Standard for Soil Test Method. China Planning Publishing House: Beijing, China, 1999; 151–173.
49. Zhao, J.; Luo, H.J.; Huang, X. Preliminary Analysis of Crystallization of Na<sub>2</sub>SO<sub>4</sub> Solution in Silicate Cultural Relics. *Stud. Conserv.* **2020**, *65*, 321–332. [\[CrossRef\]](#)
50. Gupta, S.; Terheiden, K.; Pel, L.; Sawdy, A. Influence of Ferrocyanide Inhibitors on the Transport and Crystallization Processes of Sodium Chloride in Porous Building Materials. *Cryst. Growth Des.* **2012**, *12*, 3888–3898. [\[CrossRef\]](#)
51. Qazi, M.J.; Salim, H.; Doorman, C.A.W.; Jambon-Puillet, E.; Shahidzadeh, N. Salt creeping as a self-amplifying crystallization process. *Sci. Adv.* **2019**, *5*, eaax1853. [\[CrossRef\]](#)
52. Derluyn, H.; Dewanckele, J.; Boone, M.N.; Cnudde, V. Crystallization of hydrated and anhydrous salts in porous limestone resolved by synchrotron X-ray microtomography. *Nucl. Instrum. Meth. B* **2014**, *324*, 102–112. [\[CrossRef\]](#)